Ultramicroscopy 259 (2024) 113925

Contents lists available at ScienceDirect

Ultramicroscopy

journal homepage: www.elsevier.com/locate/ultramic

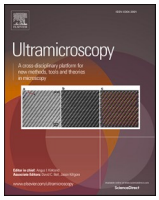

Characterization of the mechanical properties of the cortex region of human hair fibers by multiparametric atomic force microscopy mapping

Raissa Lima de Oblitas [a,*], Flávio Bueno de Camargo Junior [b], Wagner Vidal Magalhães [b], Fernanda de Sá Teixeira [a], Maria Cecília Salvadori [a]

[a] Instituto de Física, Universidade de São Paulo, São Paulo, SP 05508090, Brazil
[b] Departamento de Pesquisa, Desenvolvimento e Inovação, Chemyunion LTDA, Sorocaba, SP, Brazil

ARTICLE INFO

Keywords:
Hair fiber
Cortex region
Force curve
Young's modulus
Elastic modulus
Atomic force microscopy

ABSTRACT

We show the benefit of the use of atomic force microscopy (AFM) in spectroscopy force mode (FV: force volume) for evaluation of the cosmetic active effectiveness in improving the mechanical properties of human hair fibers cortex region. For this, we characterized human hair fibers without and with chemical damage caused by bleaching process. Fiber and resin (embedding material) data were obtained simultaneously in the mapping in order to have the resin data as a reference to ensure a coherent comparison between data from the different fiber groups. Our AFM results, which were evaluated using statistical tests, demonstrated the degradation of fibers after bleaching, corroborating the findings of transmission electron microscopy analysis and the effectiveness of a cosmetic active ingredient in improving the Young's modulus (elastic modulus) (E) of the damaged fibers. We also found a radial decrease in the natural logarithm of Young's modulus ln(E) along the cross-section of the active group fiber, which is compatible with confocal Raman spectroscopy analysis by other authors, demonstrating variation of the active permeation with depth. We note that Young's modulus was also determined by a tensile tester (macro-scale technique), in which it was not possible to obtain statistically significant differences between the groups, evidencing the advantage of the FV-AFM analysis. We also found an increase in ln(E) accompanied by a decrease in maximum adhesion force between tip and sample (negative Pearson correlation coefficient). This result can be explained by the fact that structures composed of hydrophobic components have a higher Young's modulus than structures composed of hydrophilic components.

- Bleaching damage and cosmetic hair treatment assessed by AFM, TEM, and tensile tester.
- Young's modulus by AFM nanoindentation of hair fibers monitored by sample standard.
- Young's modulus changes radially along the cross-section due to the cosmetic active.
- AFM data show statistically significant differences among sample groups.
- Tensile tester was not able to show statistically significant differences.

1. Introduction

Characterization of mechanical properties plays an important role in the development of hair care products. Sophisticated micro- and nano-scale techniques have been used to gain a better understanding of damage to the fibers caused by treatments or external agents, and to evaluate the performance of active cosmetic formulas. The search for reliable tests that provide precise and accurate data presents a constant challenge for hair fiber evaluation. Characterization of nanostructures and organization at the cellular level have been explored so as to understand the potential roles of cortex cells in determining the mechanical properties of hair [1–3].

Macro-scale characteristics, such as mechanical strength and elasticity [4,5], are determined by the internal region of the fiber, called the cortex; the cystine content (S-S bond of two cysteine amino acids) is important for these properties. The cortex is composed of cortical cells and intercellular binding material, called the Cell Membrane Complex (CMC), also present to a lesser degree in the cuticular (external) region. Cortical cells are generally 1–6 μm thick and 100 μm long aligned parallel to the fiber axis, and are the major constituent of the cortex.

* Corresponding author.
E-mail address: raissa.oblitas@gmail.com (R.L. Oblitas).

https://doi.org/10.1016/j.ultramic.2024.113925
Received 6 April 2023; Received in revised form 1 November 2023; Accepted 11 January 2024
Available online 16 January 2024
0304-3991/© 2024 Elsevier B.V. All rights reserved.

Table 2.1
– Sample specifications.

Group	Treatment
Virgin (V)	No chemical damage and no product application
Control (C)	Chemically damaged[a] and without product application
Placebo (P)	Chemically damaged[a] and with product[b] application without cosmetic active
Active (A)	Chemically damaged[a] and with product[b] application with cosmetic active[c]

[a] Chemical damage by discoloration (bleaching) from the application of hydrogen peroxide and persulfates (3 cycles).

[b] Cosmetic products: Shampoo (composed of: Water, Sodium Laureth Sulfate, Citric Acid, Cocamidopropyl Betaine, Cocamide DEA, Sodium Chloride, Xylityl Sesquicaprylate and Disodium EDTA) and a Conditioner (composed of: Water, Cetearyl Alcohol, Cetyl Alcohol, Glycerin, Cetrimonium Chloride, Xylityl Sesquicaprylate, Lactic Acid, Stearamidopropyl Dimethylamine and Disodium EDTA).

[c] Cosmetic active composed of water, Polyquaternium-7, Fibroin (silk protein) - main component of the active ingredient -, Hidroxypropyl Starch Phosphate, Glycerin and Guar Hydroxypropyltrimonium Chloride.

Cortical cells are composed of macrofibrils, which are connected by intermacrofibrillar material, cytoplasmic remnant, and melanin granules. The melanin granule determines the fiber color, according to the size and amount and type of melanin present. Macrofibrils (with diameter between 0.1 and 0.4 μm) have a substructured of intermediate filaments (with diameter approximately 7.5 nm) with low cystine content ≈6%, and a matrix rich in cystine (≈21%). The CMC consists of cell membranes and adhesive material that bind cortical cells together and consists primarily of non-keratinous protein, and has low cystine content (≈2%) [6].

The structural content can be changed by treatments or external agents. Damage caused by bleaching is common, since it is a usual step prior to dye application. Bleaching [5,7] is done using oxidizing agents, mainly hydrogen peroxide and persulfate salts. The bleaching occurs due to reaction of the oxidizing agents with melanin granules, degrading and/or solubilizing the structures, making the pigmentation color diffuse. Although the hydrogen peroxide reaction occurs predominantly with melanin granules and less with keratin [8], it is not fully selective, causing damage to other structures. The bleaching process mainly causes oxidation of cystine, generating cysteic acid, since breakdown of the amino acid cystine occurs mostly by rupture of disulfide bonds. Damage caused by oxidative processes is reflected in the chemical, structural and mechanical characteristics of the hair fiber [9].

The mechanical properties of hair fibers are typically determined macroscopically, as mentioned above. However, data obtained from macroscopic characterization does not reveal the complex ultrastructure of the fibers [10,11]. Thus, we have adopted nanoscale evaluation using atomic force microscopy (AFM).

Work has been reported using micro- and nano scale approaches – hair fiber characterization by AFM, mainly cuticle analysis [12–17]; morphological properties of the cortex region [18–20]; nanoindentation measurements and transmission electron microscopy (TEM) imaging of biological fiber cross-sections (wool) have been carried out by Parbhu, Bryson and Lal, 1999 [21], associating local measures of elasticity with ultrastructure imaging; Kitano et al. [2] have reported AFM investigation of changes in the elastic properties of human hair fiber substructure

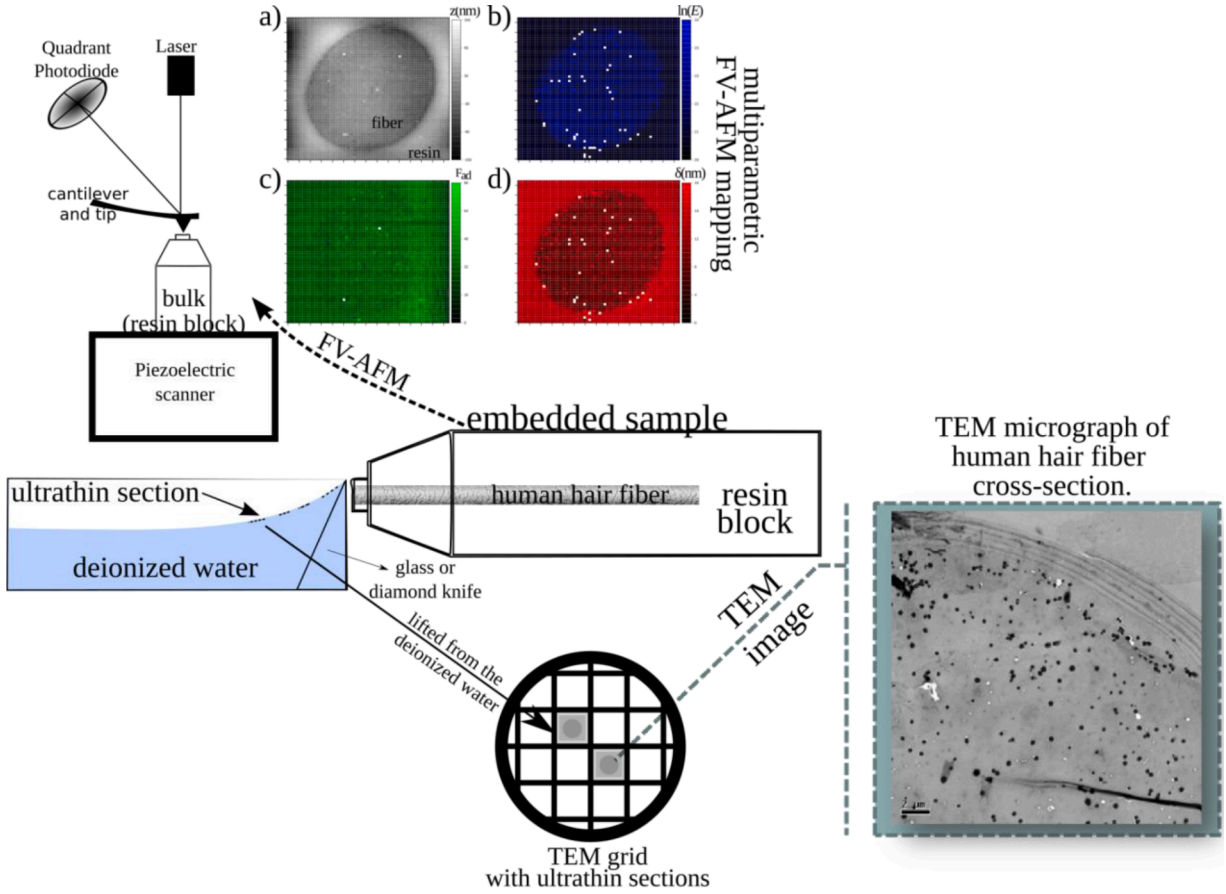

Fig. 1. Schematic representation of the sample preparation process for obtaining ultrathin sections of hair fiber embedded in epoxy resin using ultramicrotomy. An example of a TEM image (bottom-right – 2 μm scale bar) and FV-AFM maps (top-left – 72 μm × 72 μm scan size) of the hair fiber cross-section is also shown. The color scale for AFM maps corresponds to the following parameters: a) (gray scale) height values, b) (blue scale) ln(Young's modulus), c) (green scale) maximum adhesion force, and d) (red scale) sample deformation.

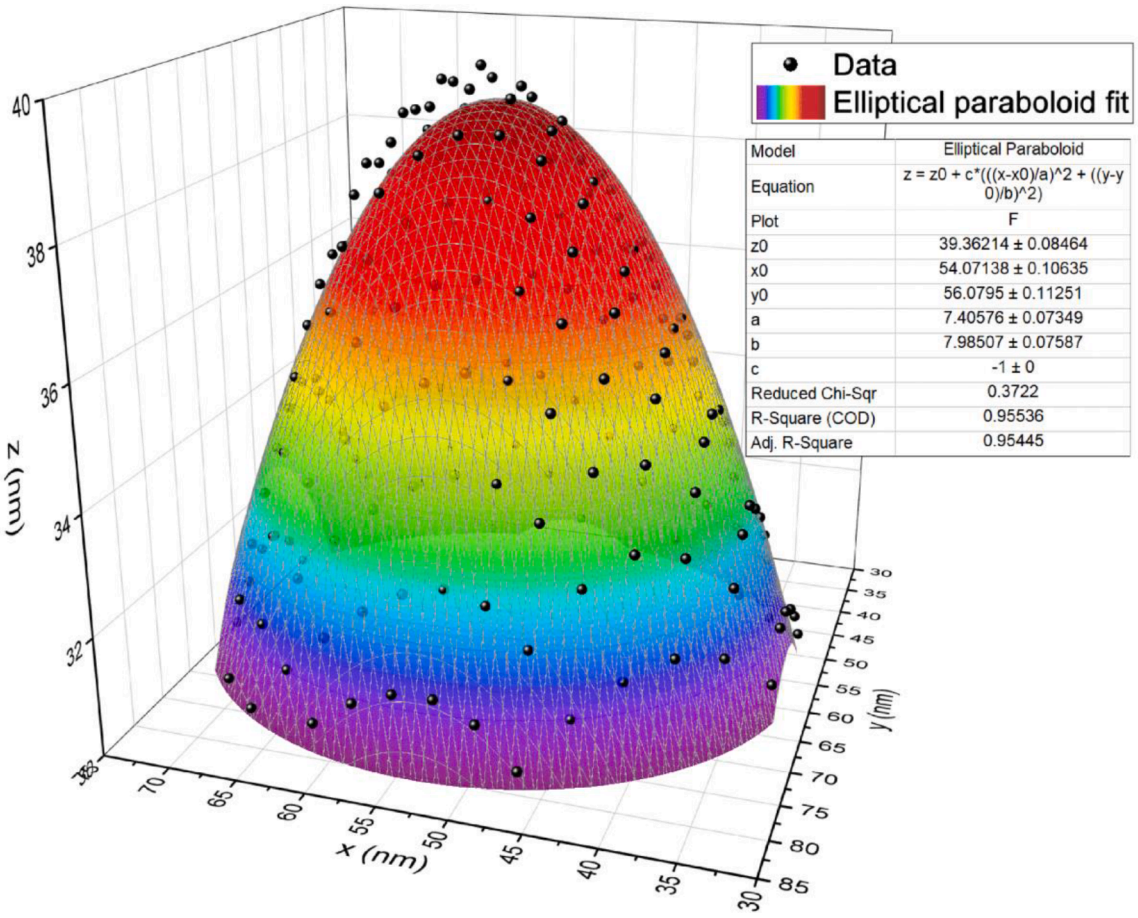

Fig. 2. Example of AFM tip data fitted to an elliptical paraboloid using OriginPro®. The black dots correspond to experimental data from the AFM tip image.

caused by chemical damage, evaluating the repairing effect of conditioning agents.

In the work described here, we have investigated hair fibers, chemically damaged or not by bleaching, with and without active cosmetic treatment. Mechanical properties of the structures were acquired collecting force curves (FC) using AFM in force volume mode. The force volume (FV) mode records a force curve [22] at each point of the sample surface scan. Surface mechanical properties on the nanometer scale were obtained by processing each curve. Young's modulus (elastic modulus) and maximum adhesion force between the AFM probe and surface were obtained, these parameters being associated with each point of the topographic image. The AFM results were correlated with macroscopic measurements (tensile tester) and TEM micrographs.

Table 2.2
– RMS roughness R_{RMS} (nm) for each sample, fitting Height-Height Correlation Function (HHCF - unidimensional), identified by treatment group (Table 2.1): V (virgin), C (control), P (placebo), and A (active) group; followed by a sample number from 1 to 8; and group average $\overline{R_{RMS}}$.

	R_{RMS} (nm)							
	V1	5.74 ± 0.04	**C1**	7.83 ± 0.06	**P1**	31.03 ± 0.27	**A1**	9.03 ± 0.04
	V2	9.09 ± 0.09	**C2**	14.80 ± 0.22	**P2**	4.616 ± 0.016	**A2**	7.01 ± 0.05
	V3	5.63 ± 0.11	**C3**	10.30 ± 0.18	**P3**	11.18 ± 0.12	**A3**	9.30 ± 0.12
	V4	4.09 ± 0.06	**C4**	15.74 ± 0.26	**P4**	51.6 ± 0.4	**A4**	29.3 ± 0.3
	V5	4.413 ± 0.010	**C5**	7.880 ± 0.022	**P5**	6.688 ± 0.016	**A5**	7.86 ± 0.03
	V6	16.7 ± 0.6	**C6**	20.9 ± 0.5	**P6**	28.06 ± 0.13	**A6**	15.04 ± 0.07
	V7	5.44 ± 0.04	**C7**	17.8 ± 0.7	**P7**	5.94 ± 0.03	**A7**	8.7 ± 0.2
	V8	3.93 ± 0.06	**C8**	9.86 ± 0.12	**P8**	8.914 ± 0.017	**A8**	7.98 ± 0.08
$\overline{R_{RMS}}$(nm)	**4.60 ± 0.25**		**8.1 ± 0.4**		**6.8 ± 1.0**		**8.6 ± 0.8**	

2. Materials and methods

2.1. Sample preparation

Samples of human hair fibers were from standardized tresses of Caucasian hair (International Hair Importers). The virgin group samples correspond to fibers without chemical damage and without cosmetic product application. Samples from the control, placebo and active groups correspond to fibers which have suffered chemical damage by bleaching (3 cycles) and were treated as in Table 2.1.

Human hair fibers were embedded in epoxy resin (STRUERS Specifix-20) and cut by ultramicrotomy (LEICA UC7 Ultramicrotome) using a glass knife to trim and a diamond knife to obtain thin cross-sections. These cross-sections were then placed on a grid for TEM observation (JEOL 1010) with beam acceleration voltage of 80 kV. To enhance contrast of the TEM micrographs, the resin block was stained with osmium tetroxide (1% per 1 h) and uranyl acetate (1% per 4 h). Additionally, ultrathin sections obtained by ultramicrotomy were stained with uranyl acetate (1% per 2 min) and lead citrate (0.2% per 1 min) to further improve the contrast. The surface of the resin block that contained the exposed hair fiber cross-section, without any staining procedures, was used for AFM characterization. Both imaging and FV mapping were performed on this surface. Fig. 1 shows a schematic representation of the procedure.

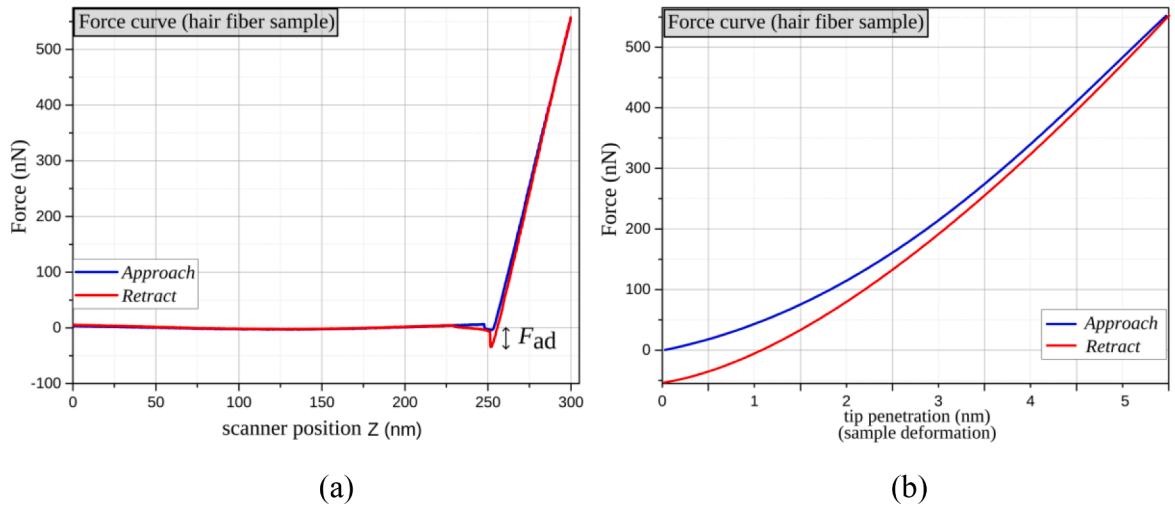

Fig. 3. (a) Example of force curve as a function as scanner position of cross-section of the hair fiber sample, showing the maximum adhesion force F_{ad}; and (b) as a function of surface deformation, showing in detail the contact region (deformation region). Blue lines represent the approach curves between surface and tip, while red lines represent the withdraw (retract) curves between surface and tip.

2.2. Atomic force microscopy analysis

AFM was performed in air using a BRUKER Multimode 8 with silicon rectangular cantilevers (NANOSENSORS PPP-NCH-W). In order to assess the mechanical properties quantitatively, we performed calibration procedures; i.e., we measured the deflection sensitivity and parameters of the probe (cantilever/tip). The deflection sensitivity (InvOLS) was obtained from a force curve on a rigid sample (Sapphire-15 M BRUKER PFQNM-SMKit). The spring constants k_c of the cantilevers used were determined by the Sader method [23,24], yielding values from 10 to 20 N/m. Tip radii were measured using a rough titanium standard sample (RS-15M BRUKER PFQNM SMKit) and fitting the tip surface as an elliptical paraboloid, yielding values from 10 to 70 nm (Fig. 2).

In order to evaluate the sample surface quality, the root-mean-square roughness R_{RMS} was obtained for each cross-section of hair fiber sample by AFM (Tapping mode) image, fitting Height-Height Correlation Function (HHCF - unidimensional) [25], according to Table 2.2.

From the data shown in Table 2.2, the average roughness $\overline{R_{RMS}} = 6.2 \pm 0.4$ nm. Note that both the average for each sample group and the average of all samples are smaller than the maximum surface deformation/indentation average $\overline{\delta_{max}} = 10.4 \pm 0.8$ nm, resulting in suitable surfaces for evaluation of mechanical properties by force curves [22].

A map of 64×64 pixels was obtained for each cross-section of hair fiber sample in force volume mode - AFM, corresponding to 64×64 force curves, of which a portion refers to curves from the resin region. A random resampling method was applied to the group dataset in order to obtain the same amount of data, so as to provide equality of variance among the different groups. The amount of data per group was determined by the group with the smallest sample size, resulting in 6214 data points from fiber region for each group, since only curves with statistical measure R-Squared $R^2 \geq 0.95$ were used. The deflection trigger was set to 40 nm. An example of a hair fiber force curve is shown in Fig. 3.

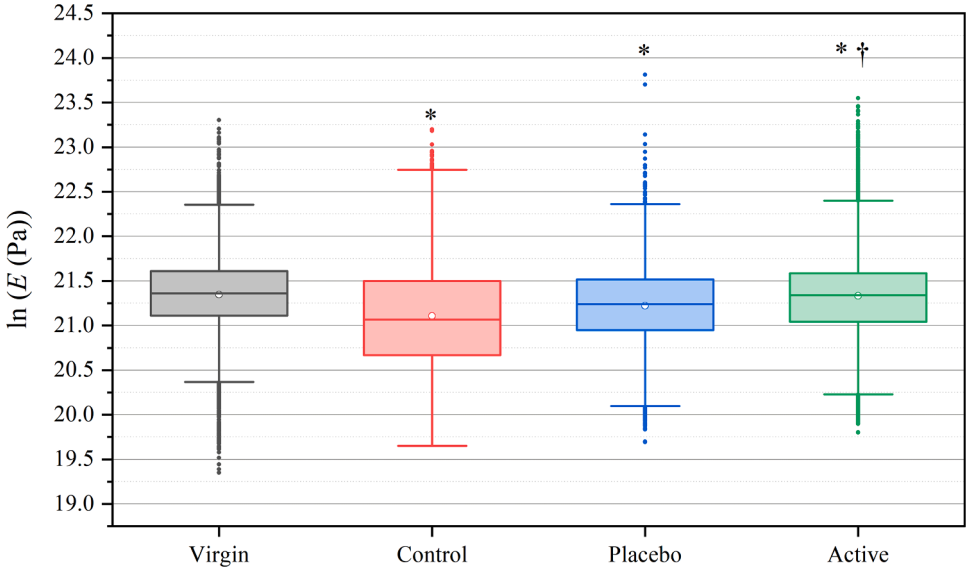

Fig. 4. Boxplots displaying ln(Young's modulus) for the different treatment groups. Statistical analysis: significance level α = 0.05 (Tukey's Multiple Comparison Test - ANOVA method).
* Statistically significant difference with Virgin group.
† Statistically significant difference with Control and Placebo group.

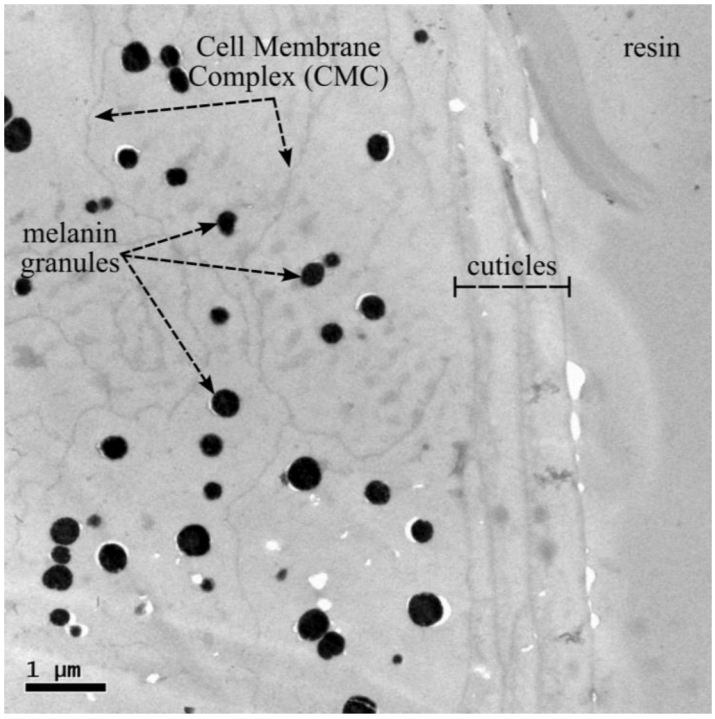

Fig. 5. TEM micrograph of 80 nm-thick hair fiber cross-section of the virgin fiber showing cuticles (external region), cortex (internal region), and resin (embedding material) regions. The arrows point to melanin granules structures and Cell Membrane Complex (CMC) structures.

The adhesion force corresponds to the point where the force begins to decrease in the retraction portion of the curve, indicating detachment of the tip from the sample due to attractive forces. To obtain Young's modulus E, it is necessary to model the relationship between the depth of indentation δ and the force applied F on the sample surface, adopting a mechanical contact model for the contact region of the force curve. In our case, the contact radius (a) could not be neglected concerning the tip radius and therefore the Hertz theory is not applicable. Thus, the Sneddon model (transcendental equation 1) [26] was used, since the ratio between maximum adhesion force and maximum load was less than 5% [27]. The curves were processed by software AtomicJ v1.8 [28], considering spherical tip radius R and Poisson ratio of the sample ν_s= 0.38 [29]. The initial contact point was automatically determined using AtomicJ software, using a 'model-independent' approach to fit the force curve during the in-contact portion and a straight-line approximation for the off-contact portion. The software finds the contact point through successive searches. The process involves minimizing the total sum of squares of the fitting of both the off-contact force curve portion and the in-contact force indentation data considering trial contact points, with the lowest sum of squares being accepted as the contact point.

$$F = \frac{E}{1-\nu_s^2}\left(\frac{R^2+a^2}{2} ln\frac{R+a}{R-a} - aR\right)$$
$$\delta = \frac{a}{2} ln\frac{R+a}{R-a} \quad (1)$$

3. Results and discussion

3.1. Analysis of the cross-section of human hair fiber

Fig. 4 shows the natural logarithm of Young's modulus ln(E) boxplot for each treatment group of the hair fiber samples. To compare the treatment groups, statistical evaluations were performed using Tukey's Multiple Comparison Test - ANOVA (Analysis of Variance) method, with significance level $\alpha = 0.05$ (5 %).

As can be seen in Fig. 4, there is a statistically significant decrease in the ln(E) mean value for chemically damaged fibers (control, placebo and active groups) and fibers without chemical damage (virgin group). This statistically significant decrease is consistent with well-established data in the literature [5], since disulfide bonds are broken in the bleaching process, resulting in loss of stiffness. The statistically significant increase in the ln(E) values for fibers of the active group (chemically-damaged and product application with cosmetic active) compared to fibers of the control and placebo groups shows the cosmetic active effectiveness, improving Young's modulus. As expected, there is no statistically significant difference in Young's modulus between the placebo and control groups, since non-activity is assumed in the placebo product.

Fig. 5 shows an example of a transmission electron microscopy (TEM) micrograph for a cross-section of virgin hair fiber, showing the external (cuticles) and internal (cortex) region, evidencing melanin granules and Cell Membrane Complex structures.

Fig. 6 shows transmission electron microscopy (TEM) micrographs for hair fiber cross-section samples belonging to the virgin and control group.

In Fig. 6a and b (virgin group micrographs) one can see that melanin granules are visualized as dark while in Fig. 7c and 7d (control group micrographs) as light, which must be holes, since the bleaching procedure degrades the melanin granules. Holes are a predominant form of damage to the cuticle and cortex of chemically modified fibers [30,31], since reactions occur not only selecting melanin granules, but also acts on other substructures as described in the Introduction, above. The same difference in contrast can be observed in the Complex Membrane Cellular (CMC). The CMC structures are visualized as dark in the virgin fiber and as light in the control fiber, evidencing the structural degradation, corroborating the Young's modulus analysis (force volume mode - AFM).

Fig. 7 shows a map acquired by AFM in the spectroscopy force mode (FV: force volume) for a cross-section of an active group fiber. Radial variation of ln(E) can be seen in the map, exemplified by two profiles traced radially along the cross section (Fig. 7), fitted by a sigmoid

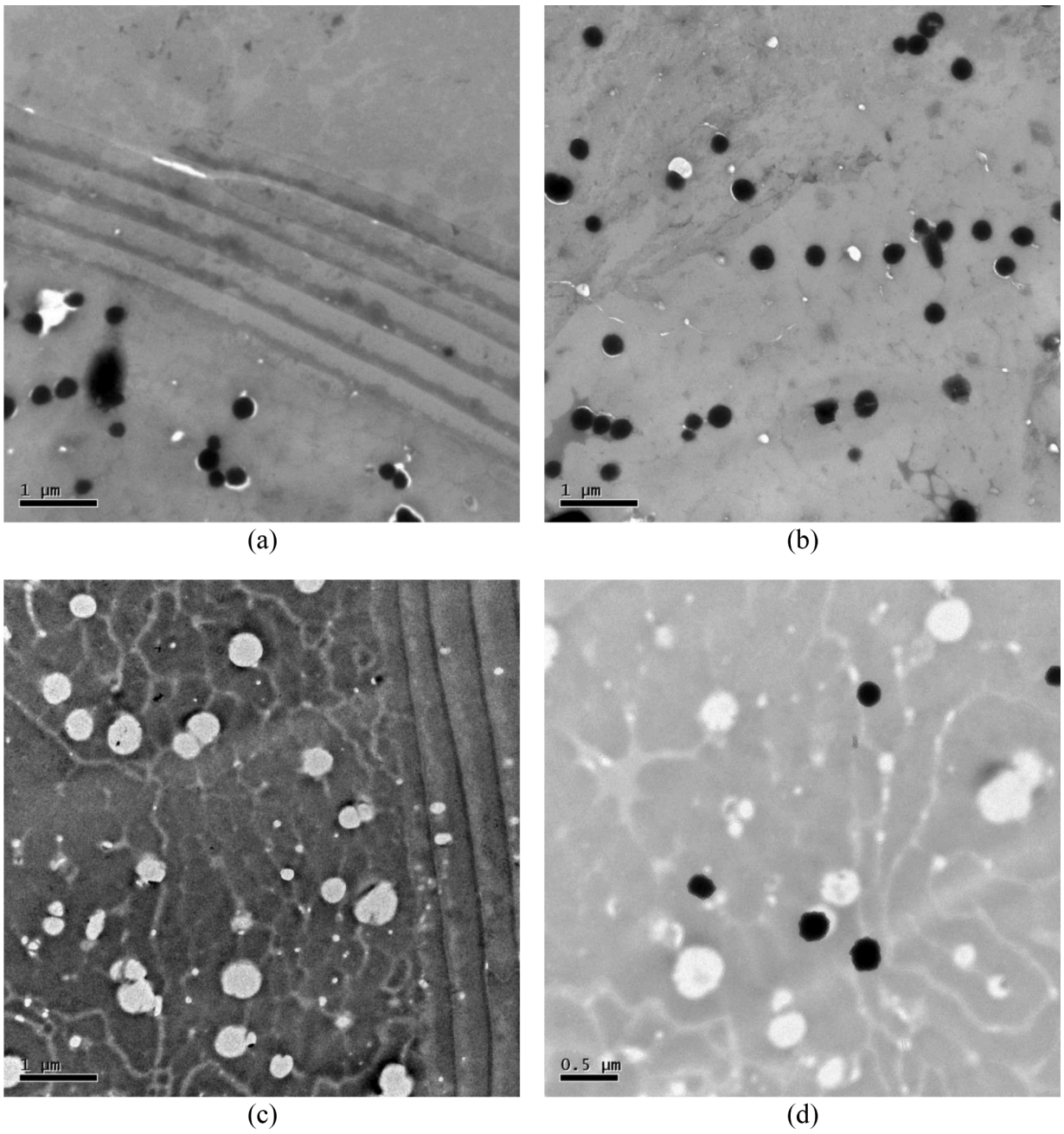

Fig. 6. TEM micrographs of 80 nm-thick hair fiber cross-section of (a)/(b) virgin and (c)/(d) control group; (a)/(c) showing the cuticles and (b)/(d) the cortex.

function. This evidences the radial permeability of the active ingredient along the fiber cross-section. Camargo et al., 2016 [32] presented a permeability study of the same active ingredient based on confocal Raman spectroscopy analysis, in which a decrease in the presence of active ingredient is reported in the region ≈ 16 µm from the edge. This finding corroborates our results, considering that the Young's modulus increase is due to the presence of the active cosmetic (Fig. 7).

Different substructures that compose the cortex have different cystine contents, which could result in different mechanical properties, as previously mentioned. Remembering that for each point on the map collected in Force Volume mode a force curve is associated, and for each curve several parameters can be extracted. Taking advantage of this, the Pearson correlation coefficient r between ln(E) and the maximum adhesion force between tip and sample (F_{ad}) (Fig. 3a) was evaluated. The Pearson correlation coefficient measures the linear correlation between two variables, ranging from −1 to 1. The closer the $|r|$ value is to 1, the stronger the correlation. Positive correlation values indicate a simultaneous increase in both variables, whereas negative correlation values indicate an increase in one variable accompanied by a decrease in the other variable [33]. Fig. 8 shows an example of a dispersion graph of ln (E) as a function of F_{ad} for a virgin group fiber. Fig. 9 shows the Person correlation coefficient r for all samples, grouped by treatments, showing the linear relationship strength for each measure.

It can be seen from Fig. 9 that the linear correlation coefficients are predominantly negative (≈72%), indicating higher values of Young's modulus for lower values of adhesion force. The prevalence of negative linear correlation coefficients can be explained by the difference between hydrophobic (lower surface energy) and hydrophilic (higher surface energy) structures. When the capillary force dominates the interaction, more hydrophilic surfaces in humid environments favor capillary condensation and liquid film formation, which can result in a significant increase in the adhesion force between surfaces [34,35].

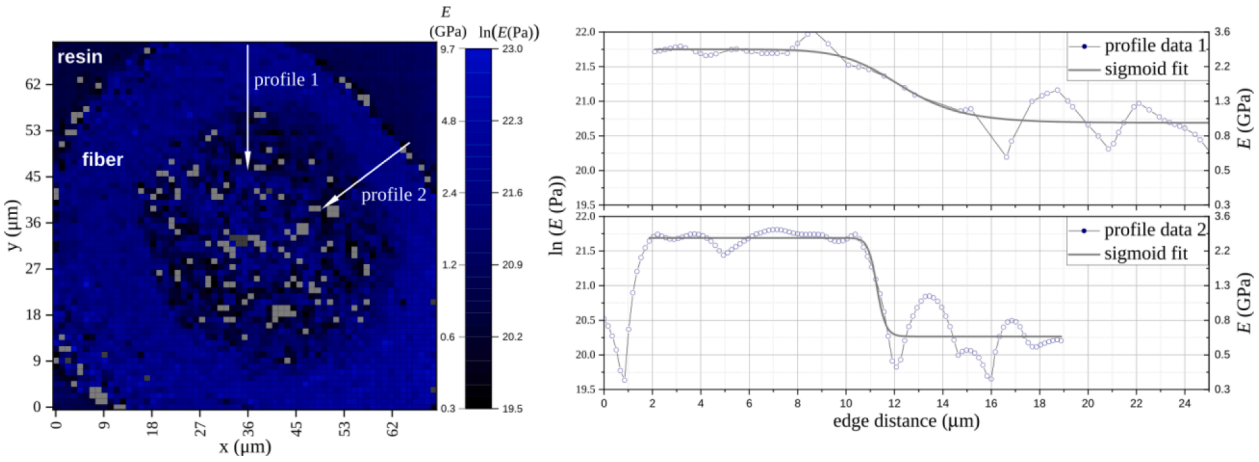

Fig. 7. Examples of profiles traced radially on the ln(E) map along a cross-section of the active group fiber, showing ln(E) as a function of distance from the edge, fitted by a sigmoid function.

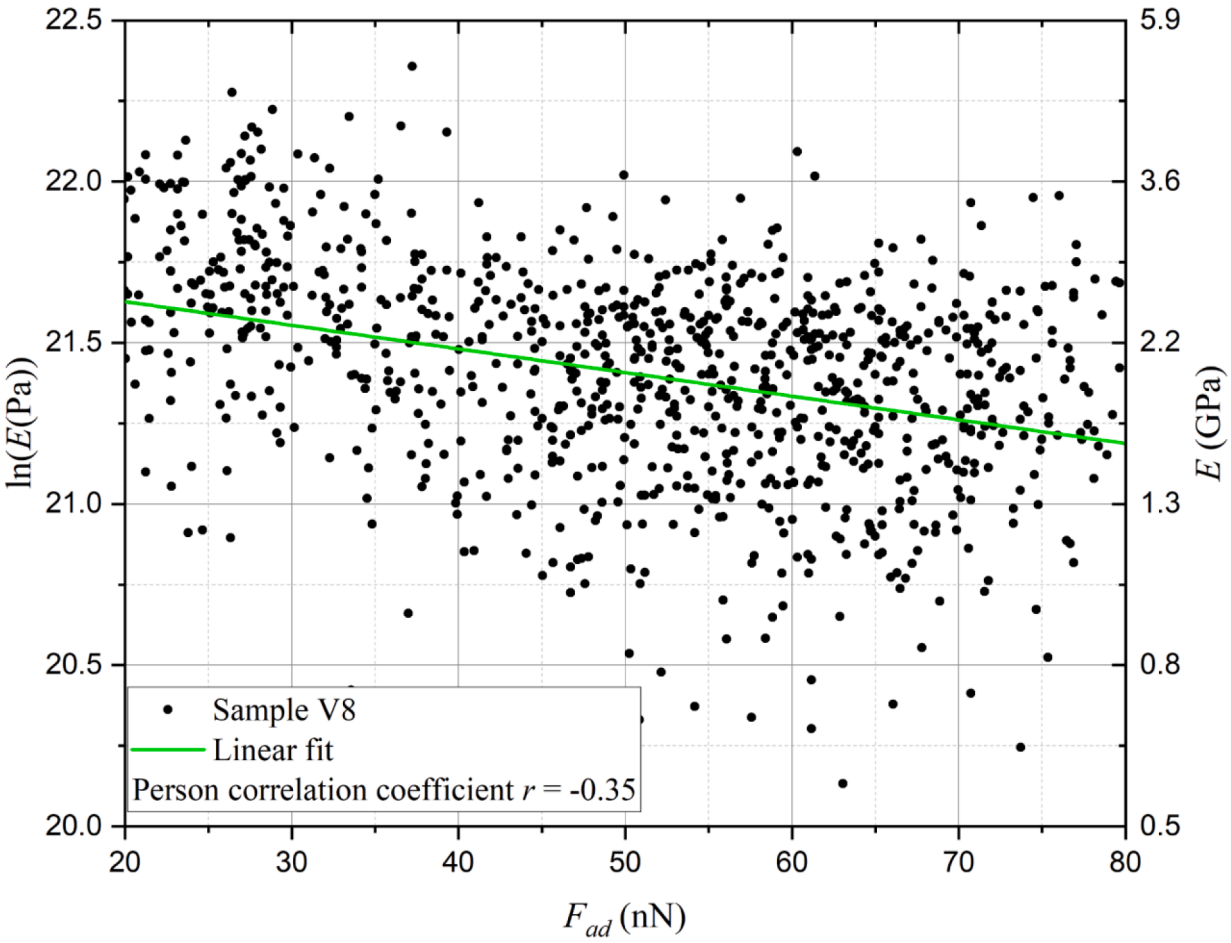

Fig. 8. Example of dispersion plot of ln(E) as a function of maximum adhesion force between tip and sample (F_{ad}), showing the calculated Person correlation coefficient r, for a virgin group fiber.

Considering this, our result agrees with Kitano et al., 2009 [2], that in general structures of hydrophilic components have a lower Young's modulus compared to structures of hydrophobic components of human hair fiber.

3.1.1. AFM versus tensile tester data

In this subsection, we describe the application of a technique in which we obtain the same parameter concerning the mechanical property of hair fiber (Young's modulus), but in macro-scale, called tensile tester. The instrument applies a controlled pulling force to the sample and records its tension response, which is the variation in its length due to sample deformation, until it breaks [36].

To obtain the Young's modulus (elastic modulus), the automated DIA-STRON MTT680 equipment was employed. Samples consisting of

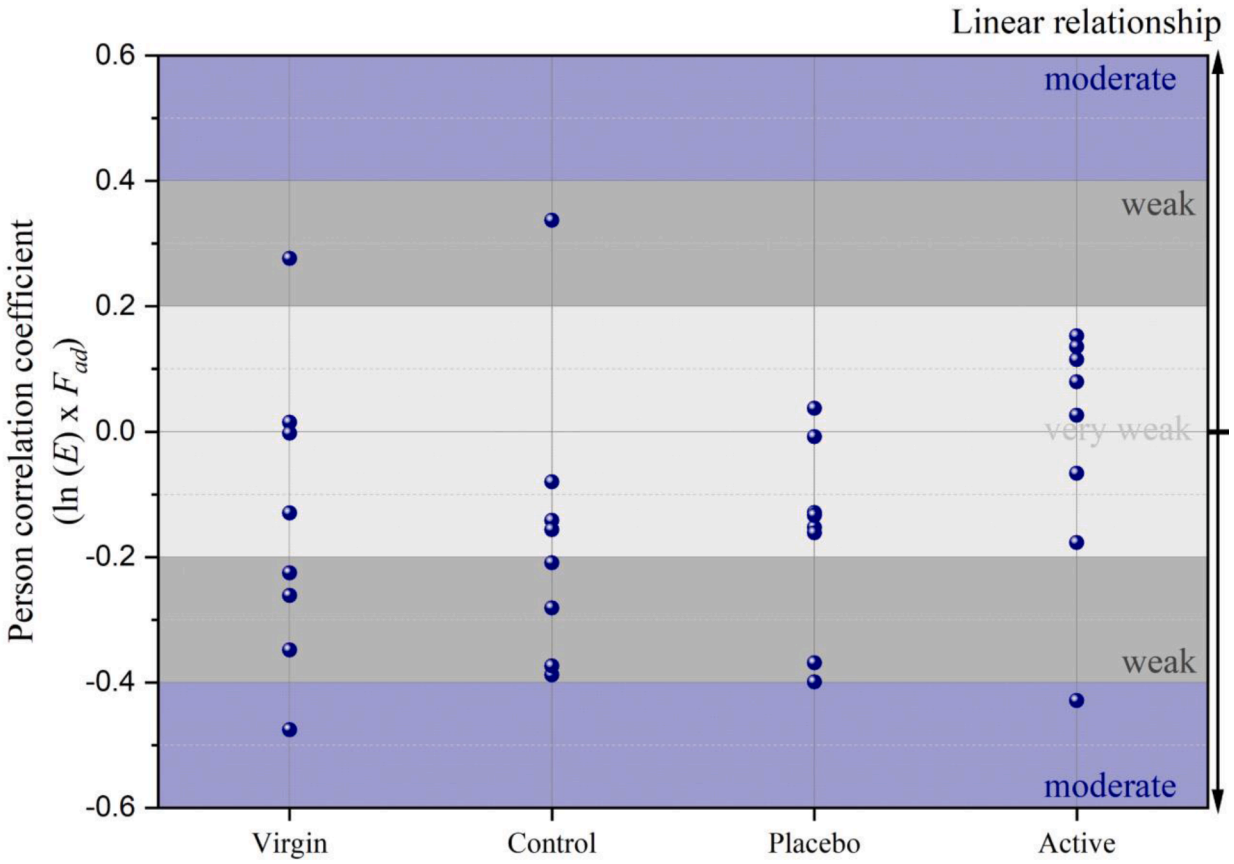

Fig. 9. Pearson's correlation coefficient *r* between ln(Young's modulus) and maximum adhesion force, for each map (sample), grouped by treatment group. Each measure was classified as very weak, weak, moderate or strong (linear relationship).

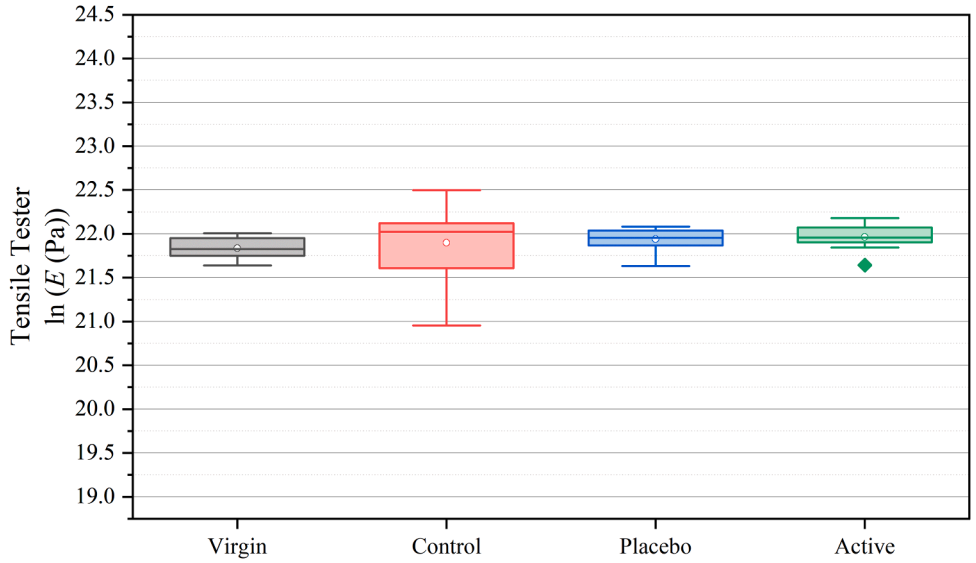

Fig. 10. Ln(Young's modulus) boxplot of measurements performed by tensile tester for each treatment group. Significance level α = 0.05 (Tukey's Multiple Comparison Test).
(No statistically significant difference).

17 fibers per group were prepared using a standard crimping block and press. Prior to the tensile test, evaluation of the dimensional properties of the fibers was conducted using the DIA-STRON FDAS770 equipment. Young's modulus for each fiber was then derived from the cross-sectional area values.

Fig. 10 shows a ln(Young's modulus) boxplot of measurements performed by tensile tester for each treatment group. To compare the treatment groups, statistical evaluations were performed using Tukey's Multiple Comparison Test - ANOVA (Analysis of Variance) method, considering the significance level α = 0.05 (5%).

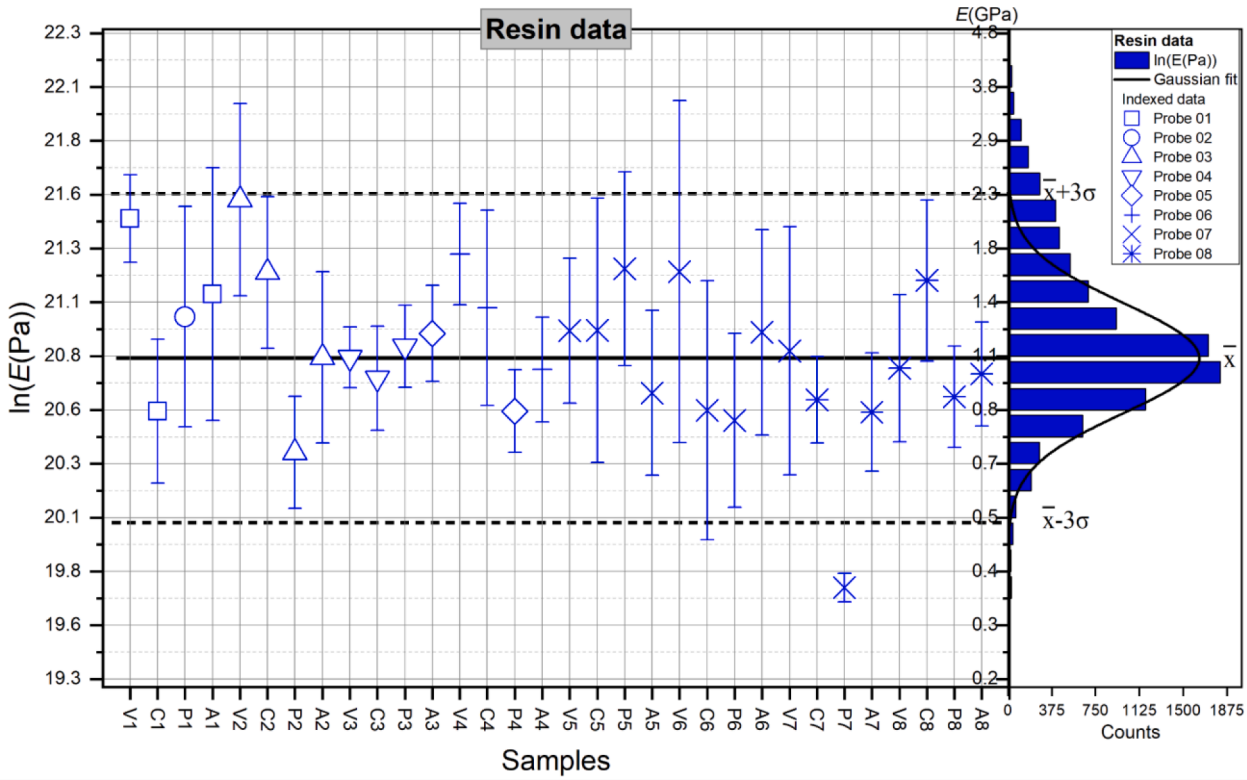

Fig. 11. (left) Average values of ln(E) and corresponding Young's modulus (E) of the resin region for each sample, indexed by probes. The solid black line represents the mean value $\bar{x}$, while the dashed black lines denote values within $\bar{x} \pm 3\sigma$, assuming a (right) Gaussian distribution for all ln(E) values.

Fig. 10 shows that there are no statistically significant differences in Young's modulus data obtained by tensile tester. Therefore, it is not possible to assess differences between the different treatment groups concerning Young's modulus, based on values obtained by the tensile tester. Since the elastic modulus is calculated from the cross-sectional area of the fiber, we note that the controlled pulling force is applied to the fiber ends and propagates to a region of a few centimeters of the fiber, and the diameter, in order to calculate the cross-sectional area, is measured at some points of the fiber using a laser scanning micrometer technique. This could be one of the sources affecting the tensile testing measurement precision. In the literature, as reported by Wortmann et al. [37], the Young's modulus of dry human hair tends to have low sensitivity to treatments. Therefore, quantification by AFM is crucial, in which statistically significant differences are found between treatment groups.

3.2. Resin data

In an ideal situation, in order to compare different samples it is desirable to use the same cantilever/tip (probe) . This procedure is usually adopted because the force curves depend on two probe parameters: cantilever spring constant k_c and tip radius R, as well as the deflection sensitivity applied in each data collection. Nonetheless, given the extent of this work we had to use several probes. Accordingly, we evaluated the resin Young's modulus data, knowing that they must be constant for all samples, since it is the same material. Thus, the resin data were monitored to ensure that the use of multiple cantilevers/tips does not interfere with comparison between the different treatment groups. Resin data were analyzed for the different probes used, even if they were of the same type. Fig. 11 shows average values of ln(E) of the resin for each sample (map) indexed by probe.

As can be seen from Fig. 11, the data show a random variation of ln (E) for the different probes used, thus confirming that the calibration procedures were performed properly. Note that this method assures a regular procedure for the use of multiple probes, as it can contain many sources of error due to several calibration steps, as reported by Schiller et al. [38].

4. Conclusions

We have demonstrated the application of AFM (force-volume mode) for the characterization of the mechanical properties of the human hair fiber cortex region. Although macroscale techniques are more widely applied to characterize mechanical properties, for instance a tensile tester, we have demonstrated that AFM offers a more accurate approach to evaluate damage and cosmetic active performance. We have also shown that it is feasible to acquire information about the structure, gaining better understanding about damage due to treatments or external agents.

We have analyzed samples without and with chemical damage caused by bleaching (virgin and control group, respectively) and chemically damaged and treated samples by product without and with cosmetic active (placebo and active group, respectively). We find that chemically damaged samples have reduced Young's modulus E (AFM results) and structural damage (TEM micrographs). The active group samples show a statistically significant increase of ln(E) between control and placebo groups, indicating the effectiveness of the cosmetic active. Young's modulus was also determined by a tensile tester (macroscale technique), with which it is not possible to identify statistically significant differences, demonstrating the advantage of AFM analysis. AFM is a technique that allows obtaining mechanical properties with high spatial resolution, as force curves can be acquired for each pixel during scanning. We also find a radial decrease of ln(E) along the cross-section (starting from the external region) for the active group sample, which suggests a radial variation of the active permeation. This result is compatible with confocal Raman spectroscopy analysis, obtained by other authors, identifying the same radial variation of the active permeation.

We observe the prevalence of a negative Pearson correlation coefficient between ln(E) and maximum adhesion force F_{ad}. This result can be explained by the fact that structures composed of hydrophobic components have a higher Young's modulus than structures composed of hydrophilic components, as found by Kitano et al. [2], considering the prevalence of capillary forces.

We conclude that systematic studies of the mechanical properties of human hair fibers using AFM, identifying nanostructures, is appropriate for cosmetic development. Effort to better understand the chemical and physical damage caused by environmental agents or treatments can elucidate interactions between cosmetic active components and internal substructures of the fibers.

Declaration of competing interest

The authors declare that they have no known competing financial interests or personal relationships that could have appeared to influence the work reported in this paper.

Data availability

Data will be made available on request.

Acknowledgments

This work was supported by the Chemyunion Ltda (Brazil) [Proj. 2427]; the Coordenação de Aperfeiçoamento de Pessoal de Nível Superior (CAPES, Brazil – Finance Code 001); the São Paulo Research Foundation (FAPESP, Brazil) [grant number 2000/08231-1]; and the Conselho Nacional de Desenvolvimento Científico (CNPq, Brazil).

We are grateful to workers at the Laboratório de Filmes Finos of the Institute of Physics, University of São Paulo (LFF - IF USP) for support throughout the experiments.

References

[1] D.P. Harland, R.J. Walls, J.A. Vernon, J.M. Dyer, J.L. Woods, F. Bell, Three-dimensional architecture of macrofibrils in the human scalp hair cortex, J. Struct. Biol. 185 (2014) 397–404, https://doi.org/10.1016/j.jsb.2014.01.010.

[2] H. Kitano, A. Yamamoto, M. Niwa, S. Fujinami, K. Nakajima, T. Nishi, S. Naito, Young's modulus mapping on hair cross-section by atomic force microscopy, Compos. Interfaces 16 (2009) 1–12, https://doi.org/10.1163/156855408×379397.

[3] C. Kunchi, K.C. Venkateshan, R.B. Adusumalli, Nanoindentation of hair cortex and medulla regions, Fibers Polym. 20 (2019) 1538–1545, https://doi.org/10.1007/s12221-019-8775-5.

[4] M. Feughelman. Mechanical Properties and Structure of Alpha-Keratin Fibres: wool, Human Hair, and Related Fibres, UNSW Press, Sydney, 1997. https://doi.10.1177/004051759706700.

[5] C.R. Robbins, Chemical and Physical Behavior of Human Hair, Springer, Berlin Heidelberg, 2012, https://doi.org/10.1007/978-3-642-25611-0.

[6] B. Bhushan. Biophysics of Human Hair: structural, Nanomechanical, and Nanotribological Studies, Springer, Berlin ; New York, 2010. https://doi.org/10.1007/978-3-642-15901-5.

[7] C. Bouillon, J. Wilkinson (Eds.), The Science of Hair Care, 2nd ed, Taylor&Francis, Boca Raton, 2005. https://doi.org/10.1201/b14191.

[8] C. Popescu, H. Höcker, Hair—The most sophisticated biological composite material, Chem. Soc. Rev. 36 (2007) 1282, https://doi.org/10.1039/b604537p.

[9] C.R.R.C. Lima, R.J.S. Lima, L.D.B. Machado, M.V.R. Velasco, L. Lakic, M. S. Nordentoft, L. Machuca-Beier, S. Rudić, M.T.F. Telling, V.G. Sakai, C.L. P. Oliveira, H.N. Bordallo, Human hair: subtle change in the thioester groups dynamics observed by combining neutron scattering, X-ray diffraction and thermal analysis, Eur. Phys. J. Spec. Top. 229 (2020) 2825–2832, https://doi.org/10.1140/epjst/e2020-900217-4.

[10] L. Kreplak, A. Franbourg, F. Briki, F. Leroy, D. Dallé, J. Doucet, A new deformation model of hard α-keratin fibers at the nanometer scale: implications for hard α-keratin intermediate filament mechanical properties, Biophys. J. 82 (2002) 2265–2274, https://doi.org/10.1016/S0006-3495(02)75572-0.

[11] E. Cloete, N.P. Khumalo, J.C. Van Wyk, M.N. Ngoepe, Systems approach to human hair fibers: interdependence between physical, mechanical, biochemical and geometric properties of natural healthy hair, Front. Physiol. 10 (2019) 112, https://doi.org/10.3389/fphys.2019.00112.

[12] B. Bhushan, C. LaTorre, G. Wei, Structural, nanomechanical, and nanotribological characterization of human hair using atomic force microscopy and nanoindentation, in: B. Bhushan (Ed.), Springer Handbook of Nanotechnology, Springer, Berlin Heidelberg, 2010, pp. 1055–1170, https://doi.org/10.1007/978-3-642-02525-9_34.

[13] J.A. Swift, J.R. Smith, Atomic force microscopy of human hair, Scanning 22 (2006) 310–318, https://doi.org/10.1002/sca.4950220506.

[14] J.M. Maxwell, M.G. Huson, Scanning probe microscopy examination of the surface properties of keratin fibres, Micron 36 (2005) 127–136, https://doi.org/10.1016/j.micron.2004.10.001.

[15] B. Bhushan, N. Chen, AFM studies of environmental effects on nanomechanical properties and cellular structure of human hair, Ultramicroscopy 106 (2006) 755–764, https://doi.org/10.1016/j.ultramic.2005.12.010.

[16] I.P. Seshadri, B. Bhushan, In situ tensile deformation characterization of human hair with atomic force microscopy, Acta Mater. 56 (2008) 774–781, https://doi.org/10.1016/j.actamat.2007.10.033.

[17] C.A. Clifford, N. Sano, P. Doyle, M.P. Seah, Nanomechanical measurements of hair as an example of micro-fibre analysis using atomic force microscopy nanoindentation, Ultramicroscopy 114 (2012) 38–45, https://doi.org/10.1016/j.ultramic.2012.01.006.

[18] N. Chen, B. Bhushan, Morphological, nanomechanical and cellular structural characterization of human hair and conditioner distribution using torsional resonance mode with an atomic force microscope, J. Microsc. 220 (2005) 96–112, https://doi.org/10.1111/j.1365-2818.2005.01517.x.

[19] B. Bhushan, Nanoscale characterization of human hair and hair conditioners, Prog. Mater. Sci. 53 (2008) 585–710, https://doi.org/10.1016/j.pmatsci.2008.01.001.

[20] R.L. McMullen, G. Zhang, Investigation of the internal structure of human hair with atomic force microscopy, J. Cosmet. Sci. 71 (2020) 117–131.

[21] A.N. Parbhu, W.G. Bryson, R. Lal, Disulfide bonds in the outer layer of keratin fibers confer higher mechanical rigidity: correlative nano-indentation and elasticity measurement with an AFM, Biochemistry 38 (1999) 11755–11761, https://doi.org/10.1021/bi990746d.

[22] H.-J. Butt, B. Cappella, M. Kappl, Force measurements with the atomic force microscope: technique, interpretation and applications, Surf. Sci. Rep. 59 (2005) 1–152, https://doi.org/10.1016/j.surfrep.2005.08.003.

[23] J.E. Sader, J.W.M. Chon, P. Mulvaney, Calibration of rectangular atomic force microscope cantilevers, Rev. Sci. Instrum. 70 (1999) 3967–3969, https://doi.org/10.1063/1.1150021.

[24] J.E. Sader, Atomic force microscope cantilevers (Calibration method of Sader), (2017). http://www.ampc.ms.unimelb.edu.au/afm/calibration.html (Accessed 11 January 2019).

[25] D. Nečas, P. Klapetek, Gwyddion: an open-source software for SPM data analysis, Open Phys. 10 (2012), https://doi.org/10.2478/s11534-011-0096-2.

[26] I.N. Sneddon, The relation between load and penetration in the axisymmetric boussinesq problem for a punch of arbitrary profile, Int. J. Eng. Sci. 3 (1965) 47–57, https://doi.org/10.1016/0020-7225(65)90019-4.

[27] B. Cappella, G. Dietler, Force-distance curves by atomic force microscopy, Surf. Sci. Rep. 34 (1999) 1–104, https://doi.org/10.1016/S0167-5729(99)00003-5.

[28] P. Hermanowicz, M. Sarna, K. Burda, H. Gabryś, AtomicJ: an open source software for analysis of force curves, Rev. Sci. Instrum. 85 (2014) 063703, https://doi.org/10.1063/1.4881683.

[29] Z. Hu, G. Li, H. Xie, T. Hua, P. Chen, F. Huang, Measurement of Young's modulus and Poisson's ratio of human hair using optical techniques, in: Fourth International Conference on Experimental Mechanics, International Society for Optics and Photonics, 2010, p. 75222Q. https://doi.org/10.1117/12.851415.

[30] D.P. Harland, J.A. Vernon, R.J. Walls, J.L. Woods, Transmission electron microscopy staining methods for the cortex of human hair: a modified osmium method and comparison with other stains: TEM staining of hair cortex, J. Microsc. 243 (2011) 184–196, https://doi.org/10.1111/j.1365-2818.2011.03493.x.

[31] M.-M. Kim, Effect of procyandin oligomers on oxidative hair damage: effect of procyandin on hair damage, Skin Res. Technol. 17 (2011) 108–118, https://doi.org/10.1111/j.1600-0846.2010.00476.x.

[32] F. Camargo, C. Pacheco, W. Magalhães, C. Nogueira, M.M. Minami, R.M. Martinez, J.C. Silva, New technology to obtain a cosmetic active with the advantage of the mechanical properties of fibroin for hair treatment, in: 29th IFSCC Congress, 2016.

[33] P.D. Ellis, The Essential Guide to Effect Sizes: Statistical Power, Meta-Analysis, and the Interpretation of Research Results, 1st ed., Cambridge University Press, 2010 https://doi.org/10.1017/CBO9780511761676.

[34] G. Chen, X. Liu. Friction dynamics: Principles and Applications, Woodhead Publishing, United Kingdom; Cambridge, MA, 2016. https://doi.org/10.1016/C2014-0-02884-5.

[35] A.J. Harrison, D.S. Corti, S.P. Beaudoin, Capillary forces in nanoparticle adhesion: a review of AFM methods, Part. Sci. Technol. 33 (2015) 526–538, https://doi.org/10.1080/02726351.2015.1045641.

[36] Instrumented indentation testing, in: H. Kuhn, D. Medlin (Eds.), Mechanical Testing and Evaluation, ASM International, 2000, pp. 232–243, https://doi.org/10.31399/asm.hb.v08.a0003273.

[37] F.J. Wortmann, J.M. Quadflieg, G. Wortmann, Comparing hair tensile testing in the wet and the dry state: possibilities and limitations for detecting changes of hair properties due to chemical and physical treatments, Int. J. Cosmet. Sci. 44 (2022) 421–430, https://doi.org/10.1111/ics.12796.

[38] H. Schillers, C. Rianna, J. Schäpe, T. Luque, H. Doschke, M. Wälte, J.J. Uriarte, N. Campillo, G.P.A. Michanetzis, J. Bobrowska, A. Dumitru, E.T. Herruzo, S. Bovio, P. Parot, M. Galluzzi, A. Podestà, L. Puricelli, S. Scheuring, Y. Missirlis, R. Garcia, M. Odorico, J.-M. Teulon, F. Lafont, M. Lekka, F. Rico, A. Rigato, J.-L. Pellequer, H. Oberleithner, D. Navajas, M. Radmacher, Standardized nanomechanical atomic force microscopy procedure (SNAP) for measuring soft and biological samples, Sci. Rep. 7 (2017) 5117, https://doi.org/10.1038/s41598-017-05383-0.